

ASSOCIATION OF ELECTROSPINNING AND 3D BIOPRINTING TECHNIQUES FOR FABRICATION OF CELLULARIZED VASCULAR GRAFTS: A PROOF OF CONCEPT

Karen Elizabeth Adarme Galvão

Geovany Candido

Paula Hayakawa Serpa

Hector Américo Barone Filho

Marcelo Napimoga

Pedro X. Rodriguez Massaguer

Ana Luiza G. Massaguer Millás

All content in this magazine is licensed under a Creative Commons Attribution License. Attribution-Non-Commercial-Non-Derivatives 4.0 International (CC BY-NC-ND 4.0).



Abstract: 3D Bioprinting and electrospinning are widely explored technologies for the reconstruction of biomimetic vascular grafts, although most studies apply them separately. The main objective of this project was to mimic vascular structure by combining these two technologies, either in tubular scaffolds or in flat membranes (cellularized patches). For this, tubular structures based on PLLA/Gelatin and flat membranes based on PLLA and PLLA/Gelatin were electrospun, in which smooth muscle (SMCs) and endothelial cells (ECs) were seeded, evaluating two deposition strategies, manual and bioprinted. Histological and cellular metabolism analyzes were performed in order to assess which of the strategies the cells adapt better to. The cellularization of the tubular structures proved to be challenging, since the migration and cell infiltration to the scaffold did not occur. In the flat membranes, there was a significant difference in viability and cell growth and infiltration in the PLLA/Gelatin fibers compared to PLLA. The comparison of manual and bioprinted methods had no impact on the metabolic activity of ECs, but on SMCs, which proved to be less viable after the possible shear stress of bioprinting. The proof of concept among the 4 adopted strategies suggests that the biofabrication of acellular tubular grafts may be a simple and less costly option for a future in vivo application. In the case of flat membranes, our results indicate that the association of bioprinting and electrospinning techniques must be a potential strategy for the biofabrication of bionic vessel patches.

INTRODUCTION

The Brazilian Cardiology Association (SBC) indicates that Non-Transmissible Diseases (NCDs) are the leading cause of death worldwide, accounting for approximately 70% of deaths globally and equivalent to over 30 million deaths per year. As these diseases are

clinically difficult to treat, 72% of deaths in Brazil are due to NCDs, of which 30% are due to cardiovascular diseases and 16% are due to neoplasm (*Brazilian Cardiology Association, 2021*).

Once medications prove to be an inefficient form of treatment, surgical intervention is the only option, specifically the gold standard autologous vascular graft (*Zoghbi et al., 2016; Eilenberg et al., 2020*). However, seeing as surgery is an invasive technique, the main limitation that surgery presents is the availability of donor sites and the increased mortality risk (*L'Heureux et al., 2007; Pashneh-Tala S et al., 2016; Zhu et al., 2020*).

Nowadays, alternative methods to surgery, which include donor cryopreserved vein grafts, such as Dacron-coated stents and synthetic polymeric protein patches composed of expanded Polytetrafluoroethylene (ePTFE), are partially effective (*Jang et al., 2020*) and have been used as conduits in the reconstruction of vascular defects (*Jang et al., 2020; Pashneh-Tala et al., 2016*). However, in addition to the mechanical incompatibility of these materials, their application in small diameter vessels (less than 6mm) is limited and the rates of postoperative thrombosis (surpassing the 30% rate observed in femoral vein lesions), stenosis, anastomotic intimal hyperplasia, aneurysma formation, infections, arteriosclerosis progression and acute thrombogenicity are still high (*Isenberg et al., 2006; Hibino et al., 2015; Yamanaka et al., 2018*).

Considering the aforementioned, tissue engineering presents an excellent strategy to address the limitations observed, given that it uses materials and cells organically (*Isenberg et al., 2006; Zhang et al., 2018; Liu et al., 2020*). 3D bioprinting and electrospinning are technologies that stand out in the field of biofabrication. 3D bioprinting, an additive manufacturing technique, has the potential to

generate layered structures with hierarchical spatial control of hydrogels and cells (Murphy & Atala, 2014). Electrospinning produces continuous polymeric fibers, natural or synthetic, in nano-or-micro-metric diameters with excellent mechanical properties.

Cui *et al.* used a coaxial 3D bioprinting system to produce bilayered tubular structures, where the internal layer was composed of human umbilical vein endothelial cell (HUVEC)-enriched Ca²⁺ pluronic bioink and the external layer composed of smooth muscle cell (SMC)-enriched bioink containing catecholamines and methacrylated gelatin (GelMa). Both *in vitro* and *in vivo* studies showed that these reconstructed structures demonstrated good biocompatibility (Cui *et al.*, 2019). Even though hydrogels, as with other materials used in 3D bioprinting such as fibrin, collagen, gelatine and alginate, have a good biocompatibility, their low mechanical resistance makes mimicry of vascular walls and sutures difficult (Cui *et al.*, 2017).

Electrospinning has proven to address the mechanical resistance limitation efficiently (Yang *et al.*, 2019; Stefani *et al.*, 2016). Nano or microspun structures have shown great clinical application potential, as their architecture mimics the Extracellular Matrix (ECM) and due to their large surface area and high microporosity, these structures demonstrate good adhesive, migration, proliferative and cellular differentiation properties. However, the hydrophobic polymers that are largely used in electrospinning, polycaprolactone (PCL) and the poly-L-lactic-acid (PLLA), pose a challenge to cellular infiltration and biointegration of the bioink through fibrous scaffolds (Pires *et al.*, 2015). The functionalization of these polymers and scaffolds addresses the hydrophobicity challenge either through mixing the pre-electrospun hydrophilic polymers with collagen, gelatin or fibrin, or through the

surface treatment of the post-electrospun fibrous matrix (Liu *et al.*, 2020). The electrospinning technology itself allows a modification of the matrix surface as an efficient and economical technology.

Liu *et al.* (2020) used functionalized PLLA fibers with gelatin, above which they grew endothelial cells (ECs) and SMCs for urethral reconstruction. The study compared infiltration and cellular proliferation in varying PLLA and gelatin concentrations, obtaining the best results at a 75/25 PLLA/gelatin ratio.

The present study proposes a new approach to the biofabrication of tubular structures and cellular, as well as decellularized, vascular patches using a hybrid electrospinning-3D printing technology. A rotating interchangeable system between the two technologies was used to bioprint tubular structures whereas, to generate patches, a bioprinting system was implemented to layer cells above the electrospun membranes. The electrospun PLLA-based matrix provides good elasticity and, with gelatin, allowed fiber functionalization which benefitted adhesion and cell migration. A flat monolayer of bioprinted bioink cells on the surface of the PLLA matrix was performed.

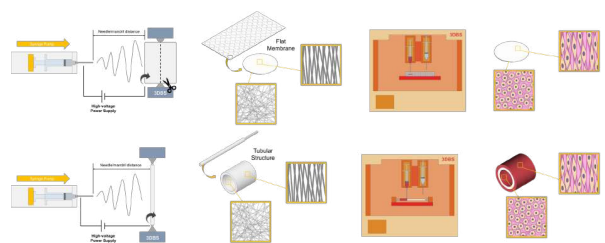


Figure 1. Schematic showing the novel approach for fabricating bionic vascular patches and tubular vascular tissue by combining rotary electrospinning and bioprinting.

MATERIALS AND METHODS

The present study used the **STARTER™** electrospinning equipment model (3D Biotechnology Solutions/Brazil), composed of: (1) voltage source in series with two electrodes positioned between the polymeric solution ejection site, and the collector, (2) an infusion device (pump) to eject the solution contained in the syringe attached to a needle with its tip cut perpendicular to its longitudinal axis and (3) an aluminum rotating collector device for the elongation and alignment of the deposited fibers (Fig. 1).

The **GENESIS™** bioprinter model (3D Biotechnology Solutions/Brazil), which is compatible with the 3D bioprinter open access code and controlled by the Marlin firmware with RAMPS1.4/Arduino electronics, was used in this study. This bioprinter contains a fourth rotating axis whose speed is optimal for the production of tubular structures (6mm diameter).

Both equipment communicate in a hybrid fashion, allowing the simultaneous presence of electrospun fibers and cell-containing bioink in the same bioconstruct (Fig. 2). In this case, two electrospun structure layouts were evaluated: 1) tubular structures (TS) and 2) patches, or flat membranes (FM).

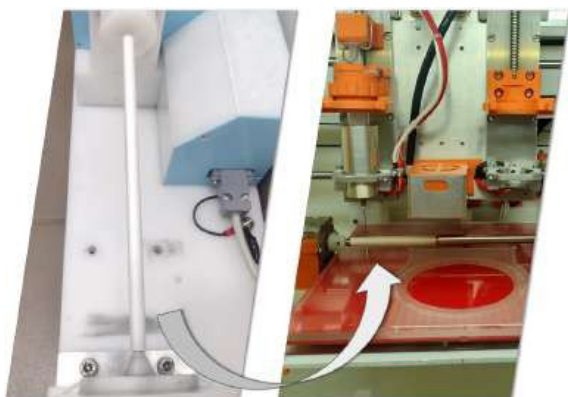


Figure 2. Hybrid System. Left image: *Electrospinning Starter™*. Right image: *Genesis™*. ELECTROSPINNING STARTER™ (3dbiotechnologiessolutions.com)

PREPARATION OF ELECTROSPINNING SOLUTIONS

PLLA and PLLA/gelatin solutions were prepared by dissolving the PLLA or PLLA/gelatin in 1,1,1,3,3,3-hexafluoro-2-propanol (HFIP) (Sigma Aldrich, USA). The PLLA/Gelatin mixtures were composed of a 75:25 proportion of the polymers. The solutions were homogenized at room temperature on a magnetic stirrer for two consecutive days. The polymeric composition, as well as the solution concentration and volume are shown on Table 1.

ELECTROSPINNING PARAMETERS

The tubular fibrous matrices and the patches were generated on rotating collector devices of 6mm and 90mm in diameter, respectively. The solutions were loaded into 10mL Luer Lock plastic syringes, coupled with descartable irrigation needles (non-bevel tips).

The tubular structures were divided into three fabrication groups (TS1, TS2 and TS3) and four membrane groups (FM1, FM2, FM3 and FM4). The established process parameters are indicated on Table 1. The samples from two groups TS1 and TS2 were generated at a 50°C, whereas variables such as temperature and air humidity were not monitored for the remaining samples.

BIOPRINTING PARAMETERS

In order to print the Tubular Structures (TS), the samples were coupled to the rotating axis of the bioprinter where two layers, each of 0.5mm in height, were deposited onto the outer layer at a speed of 40 mm/min.

The customized helicoid deposition process was developed to generate the Flat Membranes (FM) in well plates. In this deposition process, the bioprinter print head traces a helicoidal trajectory at a 600 mm/min speed, starting at the bottom of a well

Sample group	Layer	Needle (G)	Polymeric base	Concentration (% w/w)	Volume (mL)	Distance (cm)	Rotation speed (RPM)	Voltage (kV)	Flow rate (mL/h)	
Tubular Structures (TS)	TS1	Monolayer	22	PLLA/Gelatin	7,5	6	18	1000	13,3	3,5
	TS2	Monolayer	18	PLLA/Gelatin	15	3	16	5000	13,3	3,5
	TS3	Inner layer	25	PLLA/Gelatin	7,5	1,6	18	1000	12,5	0,5
Outer layer		22	PLLA/Gelatin	15	1,6	16	6000	13	1	
Flat Membranes (FM)	FM1	Bottom layer	25	PLLA	7,5	4	16	2000	9,7	3
		Top layer	21	PLLA	25	2	16	3450	12,7	0,8
	FM2	Bottom layer	22	PLLA/Gelatin	7,5	4	16	600	12,5	3
		Top layer	22	PLLA/Gelatin	12	10	16	3300	9,9	3
	FM3	Bottom layer	25	PLLA	7,5	4	16	2000	10,5	3
		Top layer	22	PLLA	20	8	10	2950	10,4	3
	FM4	Bottom layer	25	PLLA/Gelatin	6	4	14	2000	10,7	3
		Top layer	22	PLLA/Gelatin	12,5	12,5	10	2900	10,4	3

Table 1. Established parameters for the generation of tubular structure and electrospun membranes.

and ending at the top, thus distributing the precursor solution homogeneously above the samples. Both deposition processes used sterile 22G needles with straight tips.

DEVELOPMENT OF FLAT BILAYERED BIONIC MEMBRANES

For the development of bionic matrices, the behavior of ECs and SMCs were compared when cultured above PLLA fibers versus PLLA fibers functionalized with gelatin (75/25), referred to as PLLA/Gelatin (Liu., 2018). The proliferation and infiltration behaviors were evaluated qualitatively, and the cellular metabolism was evaluated quantitatively.

CELL CULTURE

The smooth muscle cells (SMCs) (A7r5, BCRJ/Brasil) and human endothelial cells (ECs) (EA.hy926, BCRJ/Brasil) were cultured in DMEM High Glucose (D7777, Sigma), with 10% fetal bovine serum (FBS) (12657-026, Gibco), 1% penicillin (100 units/mL) and streptomycin (100 µg/mL). The culture medium was changed every two days and the cells were expanded with EDTA-trypsin once they were 90% confluent.

ALGINATE AND GELATIN BIOINK PREPARATION

The 6% alginate hydrogel (w/w) (W201502, Sigma) and 4% bovine gelatin (w/w) (48723-500G-F, Sigma) were prepared in house. For guaranteed homogenization, Phosphate Buffered Saline (PBS) 1x and alginate were added in small volumes and interspersed to a schott bottle. The hydrogel was placed in a 50 C water bath and on the magnetic stirrer until completely homogenous. The water bath temperature was altered to 45 C and the bovine gelatin was added until the solution was fully homogenized. The hydrogel remained still, in room temperature, for two days after which it was stored at 4C until retrieved for use.

EXPERIMENT DESIGN AND EVALUATED STRATEGIES

Four strategies were evaluated involving combinations of electrospinning and 3D bioprinting techniques. These strategies differed based on the direction and sense of the “cellular migration” vector towards the top of the sample and based on sample type (Tubular Structures, TS, or Flat Membranes, FM), and they are labeled according to the sample position, that is: Inside vertically, Outside vertically and Half tube - for the Tubular Structures (TS); and Flat for the Flat

Membranes (FM) (Figure 2).

The Inside vertically (Fig. 5A) and Outside vertically (Fig. 5B) strategies tested cellular migration perpendicular to gravity (decantation sense) and from precursor solution to the top of the sample, migrating externally and internally, respectively. Inversely, the samples in the Half (Fig. 5C) tube strategy were cut in a canoe shape and placed convex-face up, where the precursor solution is added to coincide the migration direction with that of cellular decantation.

It is important to be careful while peeling samples off the aluminum foil so as to not dismember them, and spray 70% ethanol on them prior to removing them. For the Flat strategy, the membranes were cut with a circular 15mm diameter punch and placed in 24-well plates with the surface of interest (top layer or bottom layer) faced up. Therefore, the decantation sense, as well as in the Half tube strategy, will favor cellular migration. However, to prevent the floating and inverting of samples, and to avoid cellular leak to the bottom of the well and to the side of the membrane faced downwards, the samples were locked to the well using PLA rings that were 3D printed in house (Fig. 7B).

All samples were sterilized in house with 70% ethanol and UV-light for 2 hours, inverting the sample side after the first hour.

Before the process, some groups were pretreated in either a PBS or media bath and were incubated in this phase for three days.

The cells of interest were trypsinized and centrifuged for 3D cell culture. The supernatant was discarded and the pellet was resuspended in High Glucose medium. The cells were counted in the Neubauer chamber and were then homogenized into the precursor solution.

Two deposition methods were evaluated (manual and bioprinted) as well as two precursor solutions (hydrogel and media).

During the media manual deposition, cells were resuspended with each suction, whereas when working with hydrogel and media bioprinting deposition, the cells were homogenized in the precursor solution only at the start of the process.

After the bioink deposition, the hydrogel was reticulated with calcium chloride for three minutes, washed with PBS once, and only then received culture medium. Regarding the deposition of cells with media (precursor), 400 μ L of medium was added initially and after a 3 hour incubation more medium was added to fill the well volume.

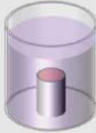



The evaluated strategies, as well as the experimental design diagram, with sample groups, deposition methods, precursor solution, sample pre-treatment, cell type and cell count per well, are indicated on Figure 3.

SCANNING ELECTRON MICROSCOPY (SEM): FIBER MORPHOLOGICAL CHARACTERIZATION

The samples were submitted for SEM at the Calibration and Analytical Resources Laboratory/UNICAMP (LRAC/UNICAMP). 40 fibers were selected for measurement. The diameters of the fibers and pores were analyzed using the *ImageJ* software. The orientation of the fibers was analyzed with the same software but with the *OrientationJ* plugin (Connor, Cahill and Mcguinness, 2021).

HISTOLOGICAL ANALYSIS

Flat Membranes samples were fixed in formaldehyde (4%) for two hours, washed twice with PBS and later stored in 70% ethanol until analyzed. Two types of analysis were performed: (1) Cross-Section: histological sections with paraffin were stained with hematoxylin and eosin (H&E). The sections, which were 4 μ m in thickness, were made with the microtome. (2) Panoramic View: the membranes were stained

Evaluated strategy	Diagram	Sample group	Deposition method	Precursor solution	Sample treatment	Cell Type	Cells/Well
Inside vertically		TS1	Manual	Hydrogel	N/A	ECs	1,8*10 ⁵
Outside vertically		TS2	Bioprinted	Hydrogel	N/A	SMCs	1,8*10 ⁵
Half tube		TS1; TS3	Manual	Medium	Medium bath	SMCs	4*10 ⁴
			Manual	Medium	PBS bath	SMCs	4*10 ⁴
			Manual	Hydrogel	Medium bath	SMCs	7*10 ⁴
			Manual	Hydrogel	PBS bath	SMCs	7*10 ⁴
Flat		FM1; FM2	Manual	Medium	N/A	ECs; SMCs	10 ⁴ ; 10 ⁴
		FM3; FM4	Manual	Medium	PBS bath	ECs; SMCs	10 ⁴ ; 4*10 ⁴
			Bioprinted	Medium	PBS bath	ECs; SMCs	10 ⁴ ; 4*10 ⁴

Sample
 Precursor solution
 PLA ring
 Culture medium

Figure 3: Experimental design and evaluated strategies for the combination of electrospinning and 3D bioprinting.

superficially with H&E.

The slides were prepared with biological resin and observed in a light microscope (Leica).

IMMUNOFLUORESCENCE STAINING

Flat membranes FM1 and FM2 were removed from 70% ethanol and washed with PBS 1x. The samples were permeabilized with 0.5% Triton X-100 for 10 minutes and incubated at room temperature in a blocking buffer consisting of PBS 1x with 5% skimmed milk (Molico) for 30 minutes. The samples were washed three times with PBS and incubated with antibodies. Bottom layers were incubated *overnight* with VWF antibody (F3520 Sigma) after which they were washed with PBS three times and incubated with the secondary antibody Alexa 488 (A-11001 Invitrogen) for two hours in the dark.

Top layers were incubated with α -SMC (C6198 Sigma) in the dark for 30 minutes at room temperature and 30 minutes at 4C. The samples were observed under a fluorescence microscope (ZEISS).

METABOLIC ASSAY (PRESTO BLUE)

Cellular viability was evaluated with Presto Blue. The media was removed from the wells and 400 μ L of a 1:10 Presto Blue (Invitrogen A13262) dilution in DMEM was added to each well. The plate was covered with aluminum foil and incubated at 37C for two hours. After the incubation, three aliquots of 100 μ L from each well were transferred to a 96-well plate. The absorbance was measured using a plate reader (Epoch, Biotek) at a 570 nm wavelength.

STATISTICAL ANALYSIS

The *Graph Prism* software was used for quantitative analysis. The results are expressed as mean and standard deviation or error of measurement (s.e.m.). Non-parametric one sample t-tests were performed in the distribution graphs and Two Way ANOVA analysis was used to compare differences between two or more groups. Tukey's and Sidak's multiple comparisons were performed in Presto Blue absorbance measurements.

RESULTS

MORPHOLOGY OF THE TUBULAR STRUCTURES

Three types of the 6mm diameter tubular fibers were generated: random alignment monolayers (TS1), aligned monolayer fibers (TS2) and bilayer fibers (TS3) (Fig. 4A). The SEM images were used to analyze fiber morphology, measure diameters ($n = 80$ fibers/sample) and coherence. A comparative analysis was performed across all tubular samples (Fig. 4B). The samples of higher concentration (15%), TS2 and TS3 Outer, had diameters that were at least ten times larger than that of samples at a 7.5% concentration (TS1 and TS3 Inner - Fig. 3B), indicating a significant difference. The analyses also indicated a variation in the average diameter of fibers within a given group (in other words, fibers that were processed with the same parameters). In relation to fiber coherence, the greatest value obtained, of 34%, was encountered in the TS3 Outer fiber, generated at a speed of 6000 RPM, followed by 21.4% coherence in the TS2 fiber, 6.5% in the TS3 Inner fiber and 6.1% in the TS1 fiber.

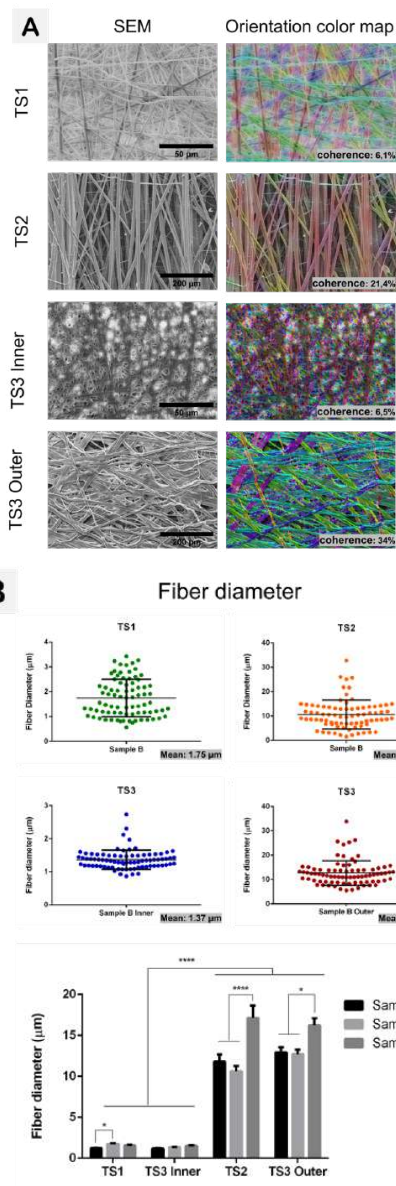


Figure 4. Morphological analysis of Tubular Structures. A) SEM images (2,000x and 500x) and B) Fiber diameter distribution graphs of TS1, TS2, TS3 Inner and TS3 Outer and comparative graph of these samples. (****) indicates $p < 0,0001$.

The panoramic view histological analysis allowed the identification of cells in only two samples, both from day 1, using the Half tube strategy (Fig. 5C) and medium as the precursor solution: (1) TS3 Outer, with sample pretreatment in media bath (Fig. 5D) and (2) TS1, with sample pretreatment in PBS bath

(Fig. 5E). After H&E staining of the bioink, cells were retained in the reticulated bioink, impeded from migrating in any direction.

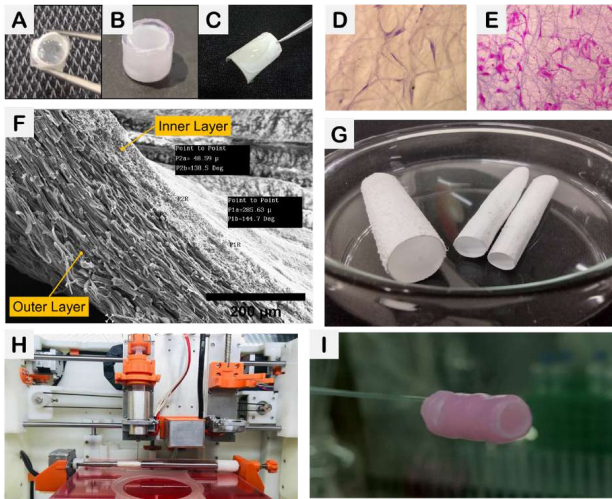


Figure 5. Tubular Structures. Evaluated strategies: A) Inside vertically; B) Outside vertically and C) Half tube. Panoramic View on day 1, Half tube deposition strategy using medium as the precursor solution; D) TS3 Outer with pretreatment in medium bath; E) TS1 with pretreatment in PBS bath; F) SEM of bilayer tubular structure. G) Macro photograph of Tubular structure. H) Bioprinting process using the hybrid system. I) Sample after bioink deposition onto the outer layer.

FLAT MEMBRANE MORPHOLOGY

The generation of bilayered Flat Membranes was possible, in that the bottom layer was composed of smaller diameter fibers and the top layer had larger diameter fibers (Fig 6A, 7E 8A).

Regarding the fiber alignment, coherences above 55% were reached with speeds starting at 2000 RPM. The FM3 and FM4 bottom membranes reached 38% and 57% coherence both at a rotation speed of 2000 RPM, while the top membranes reached 71% and 62% coherence with rotating speeds of 2900 and 2950 RPM respectively (Fig. 6A).

The average diameters of bottom membranes FM1 and FM2 were 370 nm and 1.57 μ m respectively, while those of

top layers were 3.35 and 6.23 μ m (Fig. 8A). The comparative analyses among fibers demonstrated significant differences between PLLA and PLLA/Gelatin membranes, in both the top and bottom layers (Fig. 8B), where the PLLA/Gelatin fibers reached the largest diameters when compared to those of PLLA fibers. In regards to the coherence and alignment of fibers, the top layer fibers on FM1 and FM2 reached 65% coherence, with rotating speed of 3450 and 3300 RPM respectively. On the other hand, the bottom layer fibers reached 52% on FM1 and 28% on FM2, with a rotating speed of 2000 and 600 RPM respectively (Fig. 8A).

The average diameters of the bottom layer fibers: FM3 (PLLA) and FM4 (PLLA/Gelatin) were of 630 nm and 1.20 μ m (Fig. 6B), respectively, even when using a lower polymer concentration on the FM4 Bottom layer (7.5% and 6% w/v). Such difference was also found between the top layers of FM3 and FM4, which reached average diameters of 1.5 μ m for the 20% w/v concentration (FM3) and 3.7 μ m for the 12.5% w/v fiber (FM4) (Fig. 6B).

When comparing the average diameter measurements of samples FM3 and FM4, for both the bottom and top layers, there were significant differences between PLLA (FM3) and PLLA/Gelatin (FM4) fibers. The distribution graphs demonstrate that fiber FM3 is more uniform than FM4. Furthermore, the formation of beads was observed on the FM3 bottom layer fibers, which was not seen on the FM4 Bottom fibers with a lower concentration (Fig 6A).

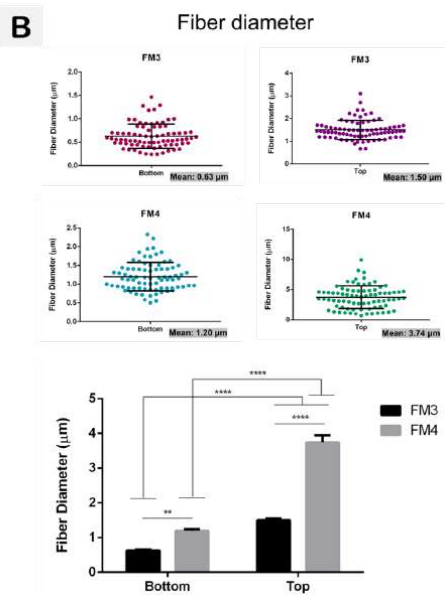
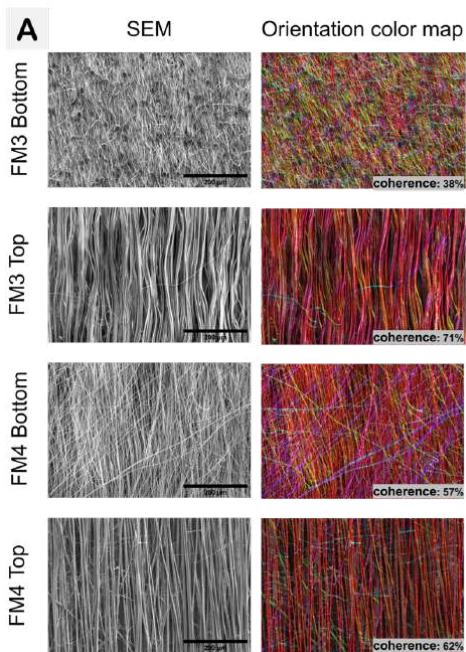


Figure 6. Morphological Analysis of Flat Membranes (FM3 and FM4). A) SEM images of bilayered Flat Membranes morphology and coherence. B) Fiber diameter distribution graphs of the bottom and top layers, with average and standard deviation (SD), and a comparative fiber diameter graph, average and standard error of measurement (s.e.m.). (**) indicates $p=0,0017$ and (****) $p<0,0001$.

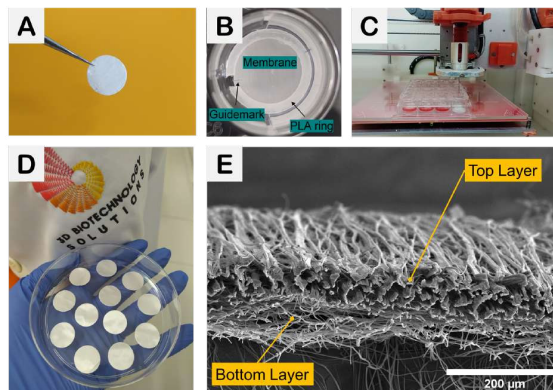


Figure 7. Flat Membranes. A) Punched sample. B) Membrane fixed with the PLLA ring at the bottom of the well. C) Bioprinting deposition method. D) Samples used in the experiment. E) SEM of the bilayer Flat Membrane.

HISTOLOGICAL ANALYSIS

In regards to the membranes, the endothelial cells (ECs) were added to the bottom layer of the fibers and the smooth muscle cells (SMCs) were added to the top layer. In the Panoramic View comparison of the ECs on fibers FM1 and FM2 (Fig. 8A), there was a greater density of ECs on day 14 on the membrane functionalized with gelatin FM2.

The top layer fibers of FM1 and FM2 stained with H&E (Panoramic View) contain a lower density of SMCs on day 14 when compared to ECs, even though the same cell count was deposited initially (10^4). No visual difference was observed in the growth of SMCs on the top layers of FM1 and FM2 (Fig. 7A). However, the immunofluorescence staining demonstrated more alpha-actin protein presence on the membrane containing gelatin, as well as a greater cell density. Furthermore, the H&E images and the immunofluorescence staining showed an elongated phenotype of the SMCs, following the direction of the aligned fibers, which suggests greater cellular differentiation.

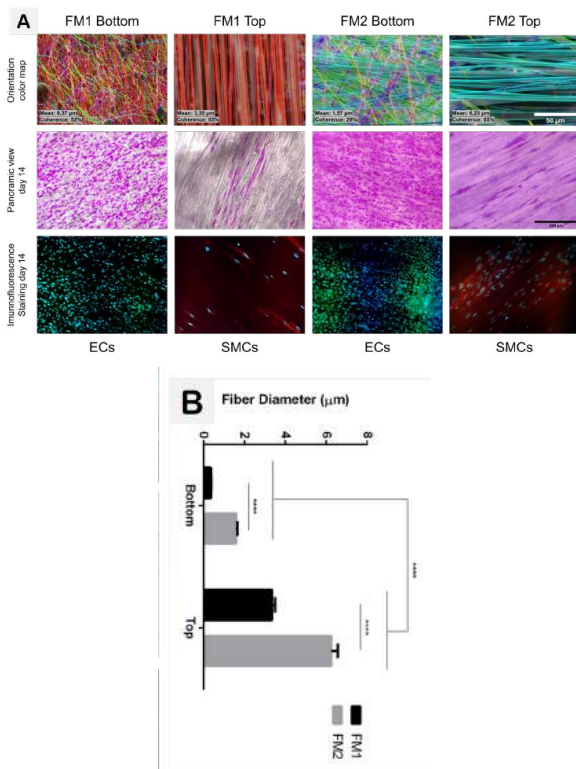


Figure 8. Experimental analysis of Flat Membranes FM1 and FM2. A) Top row: morphological characterization of fibers (SEM images and orientation color map of FM1 and FM2); Middle row: histological panoramic view (HE staining) of ECs and SMCs on day 14; Bottom row: immunofluorescent staining images on day 14, with 10 and 20x of magnitude. ECs were stained by VWF (green) and SMCs by alfa-actin (red) and both were stained by DAPI (blue) for the nuclei. B) Average fiber diameter graphs with standard deviation. (****) indicates $p < 0,0001$.

Figure 9 allows the qualitative comparison of EC and SMC cellular density on days 7 and 14 of fibers FM3 and FM4, through the Panoramic View (Fig. 9C) as well as the cross-section analysis (Fig. 9A, 9B). The H&E staining images on the Panoramic View demonstrate that ECs proliferate above both fibers, however reach a higher density on the PLLA/Gelatin fibers on days 7 and 14, when compared to the PLLA fibers. The sections show cell proliferation only on the surface of

the fibers, with no indications of infiltration, despite the greater concentration of ECs on the functionalized fibers.

The SMCs also demonstrated proliferation above both fibers, but as suggested by the images shown on Figure 9, there was higher cellular density on the PLLA fiber. Furthermore, it appears that the phenotype of these cells changed from day 7 to day 14, from elongated to a wrinkled appearance. As planned, there was greater cell infiltration on both fibers, as indicated by the arrows on Fig. 9B.

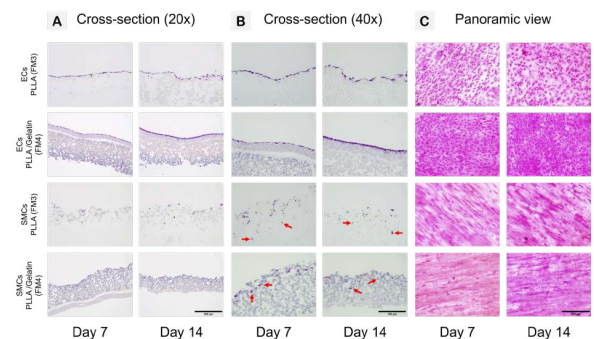


Figure 9. Histological analyses with H&E staining of ECs and SMCs on fibers FM3 and FM4 on days 7 and 14.

A) Cross-section (20x). B) Cross-section (40x) - red arrows indicate SMCs infiltration. C) Panoramic view.

Importantly, it must be noted that not only on the cross-section images, but also on the Panoramic View, PLLA fibers do not stain with hematoxylin, unlike the PLLA/Gelatin fibers. Moreover, ECs demonstrated greater resistance and adaptability to fibers when compared to SMCs, which demonstrated more fragility since the 2D culture phase.

The manual and bioprinting deposition methods were compared based on a qualitative evaluation of the growth and morphology of ECs and SMCs throughout days 1, 3, 7 and 14 post-culture (Fig. 10A, 10B). The experiment demonstrated that ECs have a star-like phenotype on day 3, specially on the

manual deposition groups. The confluency of ECs, between days 7 and 14, both on PLLA and PLLA/Gelatin membranes, is inversely proportional to the star-like morphology. However, a larger quantity of cells was observed on the PLLA membrane.

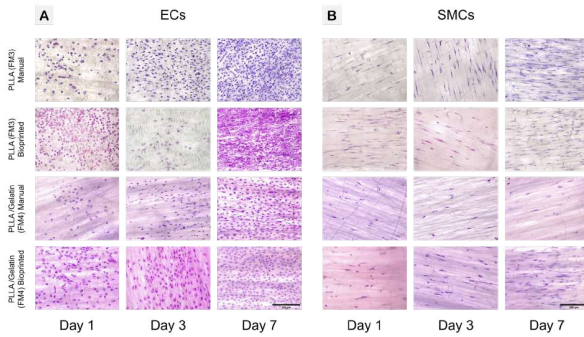


Figure 10. Histological analysis with HE staining. Panoramic view of the FM3 and FM4 fibers, with manual and bioprinting deposition of ECs (A) and SMCs (B) on days 1, 3 and 7.

In regards to the SMCs deposited either manually or through bioprinting, the cellular adhesion throughout the fiber as well as the aligned and longline morphology, was similar in all groups. Additionally, all groups except PLLA/Gelatin Manual showed greater cell density on days 1, 3 and 7.

The functionalized groups, be it manual or bioprinted, had a lower growth rate over time when compared to the PLLA groups.

ANALYSIS OF CELLULAR METABOLISM (PRESTO BLUE ASSAY)

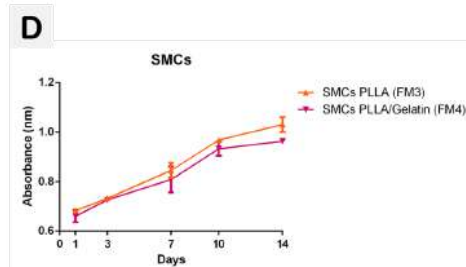
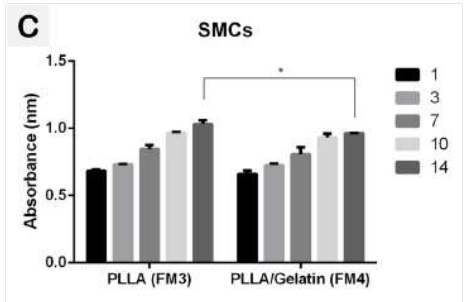
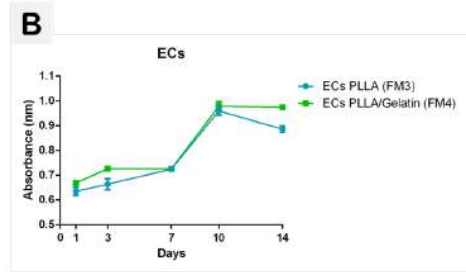
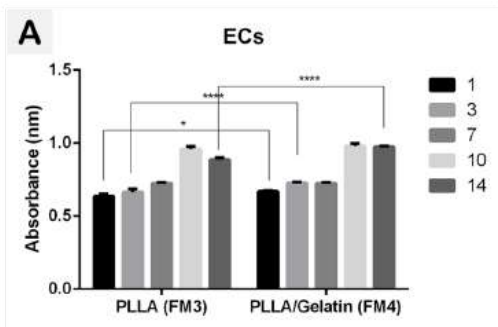


Figure 11. Flat Membranes (FM3 and FM4) Presto Blue Assay absorbances (FM3 and FM4) on days 1, 3, 7, 10 and 14. A) ECs (A) and SMCs (C) measured absorbances in PLLA and PLLA/Gelatin. Linear regressions of ECs (B) and SMCs (D). (*) indicates $p=0,0247$ and (****) $p<0,0001$. Error bars indicate standard deviation.

The metabolic activity of ECs and SMCs deposited on fibers FM3 (PLLA) and FM4 (PLLA/Gelatin) was assessed through the Presto Blue assay on days 1, 3, 7, 10 and 14 (Fig. 11).

The results indicate that ECs, on days 1, 3 and 14, were metabolically more active on the membrane functionalized with gelatin (Fig. 11A, 11B) when compared to the PLLA membrane. SMCs deposited on both fiber types showed similar cellular metabolic activity, differing significantly only on day 14, where there was a reduction in the metabolic activity of the group deposited on the functionalized

fiber versus the group deposited on the PLLA fiber (Fig. 11C, 11D).

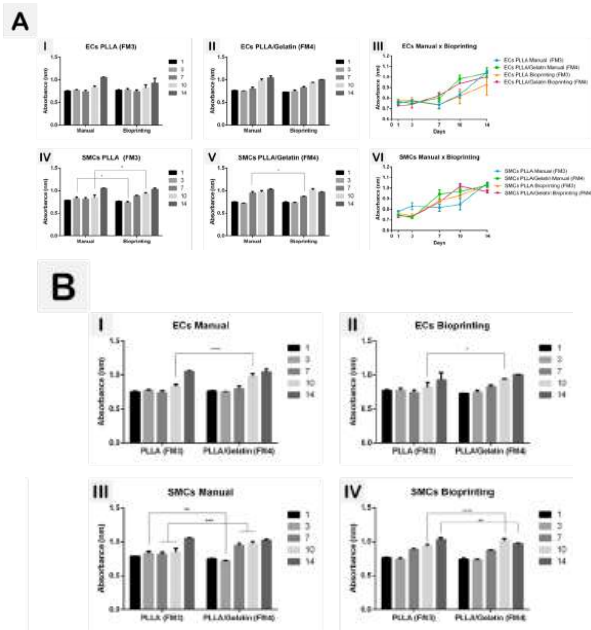


Figure 12. Flat Membranes (FM3 and FM4) Presto Blue Assay absorbances (FM3 and FM4) with ECs and SMCs deposition methods comparison (manual x bioprinted) on days 1, 3, 7, 10 and 14. A) Comparison between manual and bioprinted methods: ECs seeded in PLLA (A.I) and PLLA/Gelatin (A.II). Linear regression graph comparison of ECs (A.III). SMCs seeded in PLLA (A.IV) and PLLA/Gelatin (A.V). Linear regression graph comparison of SMCs (A.VI). B) Comparison between PLLA and PLLA/Gelatin: Manual deposition of ECs (B.I) and Bioprinted (B.II); Manual (B.III) and Bioprinted (B.IV) deposition of SMCs. (*) indicates $p < 0,1$; (**) indicates $p < 0,01$; (***) indicates $p < 0,001$ and (****) $p < 0,0001$. Error bars indicate standard deviation.

The metabolic activity was also evaluated to compare, apart from the types of fibers, the cellular deposition methods: manual and bioprinted. Cells that were deposited manually will be referred to as belonging to the Manual group, whilst those deposited with the bioprinting method belong to the Bioprinted group.

The results indicated that for ECs there were no significant differences between cellular metabolic activity when comparing deposition methods (Fig 12A. 12A.II, 12A.III). On the other hand, the results for the FM3 (PLLA) and FM4 (PLLA/Gelatin) fibers using either deposition method, manual or bioprinted, indicated that on day 10 there was greater metabolic activity of ECs on the membrane functionalized with gelatin (Fig. 12B.I, 12B.II).

SMCs showed significant differences according to deposition method and fiber type (Fig. 12A.VI). The PLLA fiber demonstrated significantly higher metabolic activity on day 3 in the Manual group whereas on day 10, the Bioprinted group had greater cellular metabolism (Fig 12A.IV). The PLLA/Gelatin fiber only showed difference on day 7 where the Manual group had significantly greater metabolic activity (Fig. 12A.V).

When comparing fibers FM3 (PLLA) and FM4 (PLLA/Gelatin), using both deposition methods (manual and bioprinted) the results indicate that on day 10 there was more cell metabolism in ECs on the fibers functionalized with gelatin (Fig. 12B.I, 12B.II). There was a greater significant difference in the Manual group when compared to the Bioprinted group. The SMCs also demonstrated metabolic activity differences between fiber types. Regarding the Manual group, the cells were more active on the PLLA membrane on day 3, whereas on days 7 and 10 cells were more active on the PLLA/Gelatin membrane (Fig. 12B.IV). Regarding the Bioprinted group, on day 10, cells were more active on the PLLA/Gelatin membrane and on day 14, there was greater cellular metabolism on the PLLA fibers (Fig. 12B.V). Therefore, these results indicate that ECs and SMCs, on day 10, regardless of deposition method, were more metabolically active on the functionalized membrane FM4.

DISCUSSION

Bioprinting and electrospinning are largely explored technologies in regards to the reconstruction of biomimetic vascular grafts, however, most studies test these separately. Nowadays, there is a strong tendency towards the combination of various biofabrication techniques, which opens a new path for biomimetic vascular tissue engineering. Thus, the present study combined electrospinning and 3D bioprinting as a hybrid system, using two approaches to develop a vascular graft: 1) tubular electrospinning scaffold structures, combined with an alginate and gelatin bioink and, 2) flat membranes cellularized with ECs and SMCs, as an alternative to vascular patches.

Both the tubular structures and the flat membranes must present specific characteristics in order to be used as cellular scaffolds, such as fiber diameter, uniformity, porosity and adequate mechanical and physical properties. Those are necessary to mimic cell extracellular matrix, enhancing cell adhesion and proliferation. In the electrospinning technique, the morphological characteristics of fibers can be controlled according to the applied production technique (Millás, 2016). In addition, the selection of polymers and solvents is also essential and influential in the electrospun matrices. For this study, despite the elevated cost, PLLA was selected as it presents a degradation rate above 12 months in the organism, a desired characteristic of tissue engineering vascular grafts and as it is an FDA approved biomaterial (Pires *et al.*, 2015). Likewise, gelatin was selected to functionalize the PLLA fibers, improving fiber hydrophilicity and generating a more cell-friendly substrate for adhesion, proliferation and migration (Rajzer *et al.*, 2018; Leyva-Verduzco *et al.*, 2020; Li *et al.*, 2022).

TUBULAR SCAFFOLDS

The three strategies used (TS1, TS2 and TS3 Outer) presented challenges related to stability of the electrospinning process, sample reproducibility, as well as challenges with cellular migration, adhesion and infiltration in the scaffolds.

The electrospinning of tubular structures in a rotating collector with a small diameter (6 mm) is shown to be challenging in the literature, as well as electrospun aligned nanofibers. Such fibers require a rotation (RPM) that is inversely proportional to the collector diameter, given that the greater the rotation, the greater the air turbulence around the chuck, which can disturb fiber alignment (Yuan, Zhou and Zhang, 2017). Furthermore, the hypothesis states that with a reduced collector diameter (6 mm) the fibers do not have enough time to stretch above the route taken during the rotation (Li and Wang, 2013; Ju *et al.*, 2017; Xu *et al.*, 2020; Leal *et al.*, 2021).

The gelatin inclusion and the wall thickness of the samples seem to have given a vitreous appearance of the samples. Gelatin was incorporated with the purpose of improving electrospun matrix hydrophilicity and improving scaffold force and elasticity properties. Otherwise, ambiental parameters such as humidity and temperature are important parameters to be controlled in the electrospinning process. Previous mechanical analyses of tubular structures were realized by BARONE in Brazil, specialized in implantable materials such as vascular prostheses. However, the results indicated stiffness, low complacency and lack of elasticity. Wall thickness was also a characteristic that may have caused the high stiffness of the samples, since the thicker it is, the more rigid it turns.

The production of bionic vascular structures using the hybrid system, which combines both the electrospinning and 3D bioprinting techniques, involves a bioink which carries

the cells to the fibrous matrix and, after reticulation, disassociates from the fiber. It was observed that cells remain reticulated in the bioink and do not migrate to the fibers in any direction, suggesting that the bioink reticulation causes cellular imprisonment. However, in the Half tube strategy, where only DMEM was used as a precursor, cells were found in only two samples (Fig. 5D, 5E).

The phenotypes of the cells differed greatly when placed in the bioink versus on the fibers. Such characteristics are directly related to the topography and biochemical composition of the environment in which these cells are located.

Initially, the purpose of the present study was to develop a cellular tubular structure (Fig 5G, 5I) capable of biointegration after implantation. However, there were several challenges in the deposition of cells in the tubular structures, which then led to the development of acellular bilayered structures. From the market, logistical and regulatory perspectives the acellular structures present advantages as they do not introduce the challenge of already containing cells within them at implantation, they are easier to generate, transport, graft and cellularize *in vivo* by the patient's own organism (Ikada, Y., 2006; Sharma *et al.*, 2019).

FLAT MEMBRANES

The bilayer membranes were generated with greater reproducibility when compared with the tubular structures. The use of the larger diameter collector (9 cm), likely contributed to the stability of the process given the larger surface area.

The PLLA flat matrices presented a more uniform topography, with round filaments whereas the PLLA/Gelatin fibers had greater heterogeneity of diameter and filament flattening (Fig. 5A, 7A). As mentioned, the humidity and temperature have an influence,

especially when working with natural polymers such as gelatin (Sell *et al.*, 2010; Bombin, Dunne and McCarthy, 2020; Keshvardoostchokami *et al.*, 2021). In the present study, these variables were not controlled, which may have led to the diversity and different morphologies of the fibers observed.

Generating homogenous fibers of a given thickness throughout the surface area of the collector was an additional challenge. Usually, most of the electrospun fiber is located on the center of the collector and less material is found laterally and towards the extremity of the collector. The horizontal movements (along the x axis) of the collector addressed this challenge. The fiber thickness was determined using a calculation based on surface area, thickness, solution concentration and time to process completion. The thickness of the fibers (about 0,3 mm) is an important factor to be considered in *in vitro* experiments and for paraffin histological sections (as it avoids section rolling and loss of samples).

In order to mimetize the morphological structure of native human vasculature, bilayer scaffolds were generated containing an internal layer composed of randomly oriented nanofibers and an external layer made of aligned microfibers. For greater hydrophilicity and cellular adhesion, the fibers were functionalized with gelatin.

The results indicate higher proliferation of ECs in the bottom layer of the functionalized fibers FM2 (Fig. 8A) and FM4 (Fig. 8C), which is likely due to the functionalization with gelatin. On the other hand, the groups Manual and Bioprinted did not follow this trend, seeing that the PLLA membranes showed greater cellular density (Fig. 10A, 10B). As discussed previously, there was more heterogeneity in the diameter of PLLA/Gelatin fibers and variation in the thickness throughout the membrane (Fig. 6B). Such characteristics may have led to different circular samples within

the same group, resulting in less proliferation of ECs. Therefore, the reproducibility of the results is still a challenge.

The morphology of ECs in flat membranes is another important aspect to be analyzed in regards to their growth and adaptability to the fibers. On polystyrene planes, these cells exhibit a star-like and elongated phenotype, with filopodia emissions. As the cells become confluent, the phenotype changes, the cells form small clusters, coming closer together and reducing their extensions. The star-like phenotype was observed, mainly on day 3 of the Manual and Bioprinted groups, in PLLA (FM3) and PLLA/Gelatin (FM4) fibers, even with significantly different topographies (Fig 10A). The flat membranes with the smallest fiber diameters (FM1 and FM3) offered a greater surface area that could favor the emission of filopodia, but they were not functionalized (Fig. 6B, 8A). In this case, functionalization seems to have a greater influence on ECs proliferation than on the topography of the fibers. Matschegewski and collaborators showed similar results when comparing the cell occupancy area and cell morphology in non-functionalized and functionalized scaffolds. Their results demonstrated that, given the same fiber topography, functionalization increased EA.hy926 density among the scaffold and the cells exhibited an elongated phenotype (Matchegewski, 2022).

Although topography and average diameter are also important features for the proliferation and phenotype of SMCs, these cells demonstrated a similar behavior as that observed with ECs. The microenvironment in aligned fibers, as seen in FM1 and FM2, may have been fundamental for the growth of SMCs (Fig 7A). Although the present study does not provide quantitative values of protein expression from the immunofluorescence assay performed, several studies demonstrate

that electrospun fibers functionalized with gelatin favor the expression of specific cell markers. A study showed that smooth muscle cells (a7r5) seeded on aligned electrospun matrices exhibited an aligned cell phenotype along the fiber and expressed higher levels of alpha-actin, which indicates a greater contractile function of these cells. The a7r5 SMCs have two phenotypes: contractile and synthetic. These phenotypes are often determined by analyzing the cell morphology. The contractile phenotype exhibits elongated and fusiform morphology, defined by the contractile filaments, which are essential for the proper functioning of a native vessel, for example. On the other hand, the synthetic phenotype exhibits a rhomboid aspect and contains several organelles responsible for synthesizing proteins (Rensen, 2017; Beamish, 2010). Studies show that, as cells are cultured over time, they can lose their contractile phenotype and present the synthetic phenotype, altering the morphology and reducing alpha-actin levels (Campbell *et al.* 1989; Campbell and Campbell, 2012).

Besides the contractile phenotype, which is specific and fundamental for possible clinical applications, cellular infiltration is also important and was one of the objectives of this study. The creation of a layer that would mimic the tunica media of blood vessels depends on the infiltration of SMC through the fiber pores, a function related to the diameter and porosity of the fibers (Pu *et al.*, 2015). One study showed that increasing the diameter of electrospun fibers reduces proliferation but increases infiltration (Han, 2019) and diameters between 7 μm or 10 μm are optimal for cell infiltration. Although our results are not in this range, evidence of SMCs infiltration was observed on the top layers of fibers FM3 and FM4 (Fig. 9A, 9B). The FM3 top layer fiber had a smaller average diameter than FM4, which would actually lead to less

infiltration of SMCs but greater proliferation on the surface. On the other hand, the FM4 top layer, with an average diameter close to 4 μ m, would lead to greater infiltration of SMCs and less proliferation. Regarding the fiber porosity, it is known that porosity is proportional to the fiber diameter, which suggests that there may have been a greater infiltration in the functionalized fiber (Millás, 2016).

Although cell proliferation and infiltration was observed, it was challenging to grow SMCs in electrospun fibers. The Panoramic View images demonstrated that smooth muscle cells proliferated less and slower than the endothelial cells. This behavior was observed in all experiments performed, even in those where the count of SMCs was 4 times greater than that of ECs.

Cellular metabolism is also an important factor for the good performance of a bionic patch. The analyses showed that functionalization with gelatin plays an important role in the metabolic activity and consequent viability of ECs and SMCs. It is known that the interaction between cells and the biomaterial is responsible for cell signaling, which regulates various functions such as adhesion, proliferation and cell viability (Matschegewski *et al.*, 2010). Studies show that the functionalization of scaffolds with gelatin is involved in improving the fiber and consequently the cellular environment, thus favoring cell growth and viability.

Cellular metabolism was also measured in the different deposition methods evaluated: manual and bioprinted, testing whether the automation of the process is an interesting approach. According to the data obtained, bioprinting metabolically did not affect ECs (Fig. 12A.I, 12A.II, 12A.III), but only SMCs on days 3, 7 and 10, with higher metabolic activity on day 10 (Fig. 12A.IV, 12A.V, 12A.VI). This may indicate stress and cellular shear at the time of bioprinting compared to manual

deposition, knowing that bioprinting involves extrusion of cells through a needle (Paxton *et al.*, 2017; Han *et al.*, 2021). The first days in culture, a time where cells are adapting to the new microenvironment and maturing, after sedimentation, seem to be more critical in the behavior of SMCs than in that of ECs.

Therefore, the automation of processes that are traditionally performed manually is of extreme importance, however it is a change that must be analyzed on a case by case basis. The present study, which combined the manual and bioprinting deposition methods in the biofabrication of vascular patches, demonstrates an interesting approach using bioprinting for the deposition of ECs and manual deposition of SMCs.

CONCLUSION

To produce multilayer morphology of a biomimetic vascular tissue, this study combined electrospinning and 3D bioprinting techniques, using two approaches to develop:

- 1) a bilayered acellular tubular scaffold and
- 2) a bionic bilayered patch membrane. Both with a random nanofibers inner layer and an aligned microfibers outer layer, by using electrospinning with PLLA and PLLA/gelatin polymers. We functionalized the PLLA fiber matrix with bovine gelatin by electrospinning and used alginate/gelatin bioink containing smooth muscle cells and endothelial cells in bioprinting to fabricate bionic vessel patches.

The artificial bilayer acellular tubular grafts using a 6 mm rotating electrospinning method was successfully constructed. Pre-cellularization of the tubular vascular grafts remains a research challenge. This method is suitable for other tubular tissue structures, such as urethra, trachea, and intestine.

Combining the advantages of these two technologies, the fabricated bionic vessel patches showed good biocompatibility. Manually deposition of SMCs showed better

results and bioprinted ECs maintained good activity, migration and function in the structure after culture. This approach may fill the need for the clinical transformation of tissue-engineered blood vessels. It could provide a new method for constructing artificial bionic tissue with both mechanical strength and biological activity.

ACKNOWLEDGMENTS

This work was supported by The São Paulo Research Foundation - FAPESP, PIPE Program (Process Number: 2019/05274-8) and the Health Innovation Hub of São Leopoldo Mandic University - HUBMandic, where the startup 3D Biotechnology Solutions is incubated. Special thanks to Prof. Dr. Elizabeth Ferreira Martinez and Mandic laboratory staff, Pollyanna Tombini Montaldi and Nadir S. de Freitas.

REFERENCES

- Beamish, J.A., He, P., Kottke-Marchant, K. and Marchant, R.E. (2010). Molecular regulation of contractile smooth muscle cell phenotype: implications for vascular tissue engineering. *Tissue Engineering Part B: Reviews*, 16(5), pp.467-491.
- Brazilian Cardiology Association (2021). <https://www.portal.cardiol.br/post/sbc-atualiza-relat%C3%B3rio-estat%C3%ADstica-cardiovascular-brasil>. [Accessed October 9, 2022]
- Bombin, A.D.J., Dunne, N.J. and McCarthy, H.O. (2020). Electrospinning of natural polymers for the production of nanofibres for wound healing applications. *Materials Science and Engineering: C*, 114, p.110994.
- Campbell, J.H., Kocher, O., Skalli, O., Gabbiani, G. and Campbell, G.R. (1989). Cytodifferentiation and expression of alpha-smooth muscle actin mRNA and protein during primary culture of aortic smooth muscle cells. Correlation with cell density and proliferative state. *Arteriosclerosis: An Official Journal of the American Heart Association, Inc.*, 9(5), pp.633-643.
- Campbell, J.H. and Campbell, G.R. (2012). Smooth muscle phenotypic modulation—a personal experience. *Arteriosclerosis, thrombosis, and vascular biology*, 32(8), pp.1784-1789.
- Cui, H., Nowicki, M., Fisher, J.P. and Zhang, L.G. (2017). 3D bioprinting for organ regeneration. *Advanced healthcare materials*, 6(1), p.1601118.
- Cui, H., Zhu, W., Huang, Y., Liu, C., Yu, Z.X., Nowicki, M., Miao, S., Cheng, Y., Zhou, X., Lee, S.J. and Zhou, Y. (2019). In vitro and in vivo evaluation of 3D bioprinted small-diameter vasculature with smooth muscle and endothelium. *Biofabrication*, 12(1), p.015004.
- Eilenberg, M., Enayati, M., Ehebruster, D., Grasl, C., Walter, I., Messner, B., Baudis, S., Potzmann, P., Kaun, C., Podesser, B.K. and Wojta, J. (2020). Long term evaluation of nanofibrous, bioabsorbable polycarbonate urethane grafts for small diameter vessel replacement in rodents. *European Journal of Vascular and Endovascular Surgery*, 59(4), pp.643-652.
- Han, S., Kim, C.M., Jin, S. and Kim, T.Y. (2021). Study of the process-induced cell damage in forced extrusion bioprinting. *Biofabrication*, 13(3), p.035048.
- Hibino, N., Mejias, D., Pietris, N., Dean, E., Yi, T., Best, C., Shinoka, T. and Breuer, C. (2015). The innate immune system contributes to tissue-engineered vascular graft performance. *The FASEB Journal*, 29(6), pp.2431-2438.
- Ikada, Y. (2006). Challenges in tissue engineering. *Journal of the Royal Society Interface*, 3(10), pp.589-601.
- Isenberg, B.C., Williams, C. and Tranquillo, R.T. (2006). Small-diameter artificial arteries engineered in vitro. *Circulation research*, 98(1), pp.25-35.

- Jang, S.R., Kim, J.I., Park, C.H. and Kim, C.S. (2020). Development of Y-shaped small diameter artificial blood vessel with controlled topography via a modified electrospinning method. *Materials Letters*, 264, p.127113.
- Ju, Y.M., Ahn, H., Arenas-Herrera, J., Kim, C., Abolbashari, M., Atala, A., Yoo, J.J. and Lee, S.J. (2017). Electrospun vascular scaffold for cellularized small diameter blood vessels: A preclinical large animal study. *Acta biomaterialia*, 59, pp.58-67.
- Khorshidi, S., Solouk, A., Mirzadeh, H., Mazinani, S., Lagaron, J.M., Sharifi, S. and Ramakrishna, S. (2016). A review of key challenges of electrospun scaffolds for tissue-engineering applications. *Journal of tissue engineering and regenerative medicine*, 10(9), pp.715-738.
- Keshvardoostchokami, M., Majidi, S.S., Huo, P., Ramachandran, R., Chen, M. and Liu, B., (2020). Electrospun nanofibers of natural and synthetic polymers as artificial extracellular matrix for tissue engineering. *Nanomaterials*, 11(1), p.21.
- Leyva-Verduzco AA, Castillo-Ortega MM, Chan-Chan LH, Silva-Campa E, Galaz-Méndez R, Vera-Graziano R, Encinas-Encinas JC, Castillo-Castro D, Rodríguez-Félix DE, Santacruz-Ortega HD, Santos-Sauceda I. Electrospun tubes based on PLA, gelatin and genipin in different arrangements for blood vessel tissue engineering. *Polymer Bulletin*. 2020 Nov;77(11):5985-6003.
- Leal, B.B., Wakabayashi, N., Oyama, K., Kamiya, H., Braghioroli, D.I. and Pranke, P. (2021). Vascular tissue engineering: polymers and methodologies for small caliber vascular grafts. *Frontiers in Cardiovascular Medicine*, 7, p.592361.
- Li, Z. and Wang, C. (2013). *One-dimensional nanostructures: electrospinning technique and unique nanofibers* (pp. 15-29). New York Dordrecht London: Springer Berlin Heidelberg.
- Li, J., Li, W., Zou, D., Kou, F., Hou, Y., Yasin, A. and Zhang, K. (2022). Comparison of conjugating chondroitin sulfate A and B on amine-rich surface: For deeper understanding on directing cardiovascular cells fate. *Composites Part B: Engineering*, 228, p.109430.
- Liu, S., Qin, S., He, M., Zhou, D., Qin, Q. and Wang, H. (2020). Current applications of poly (lactic acid) composites in tissue engineering and drug delivery. *Composites Part B: Engineering*, 199, p.108238.
- Matschegewski, C., Staehlke, S., Loeffler, R., Lange, R., Chai, F., Kern, D.P., Beck, U. and Nebe, B.J. (2010). Cell architecture–cell function dependencies on titanium arrays with regular geometry. *Biomaterials*, 31(22), pp.5729-5740.
- Matschegewski, C., Kohse, S., Markhoff, J., Teske, M., Wulf, K., Grabow, N., Schmitz, K.P. and Illner, S. (2022). Accelerated Endothelialization of Nanofibrous Scaffolds for Biomimetic Cardiovascular Implants. *Materials*, 15(6), p.2014.
- Millás, A.L.G.M. (2016). *Avaliação de propriedades in vitro e in vivo de scaffolds de PLGA incorporados com óleo-resina de copaíba preparados por eletrofição*. PhD thesis. State University of Campinas. Available at: <https://bv.fapesp.br/pt/dissertacoes-teses/155379/avaliacao-de-propriedades-in-vitro-e-in-vivo-de-scaffolds-de>
- Murphy, S.V. and Atala, A. (2014). 3D bioprinting of tissues and organs. *Nature biotechnology*, 32(8), pp.773-785.
- O'Connor, R.A., Cahill, P.A. and McGuinness, G.B. (2021). Effect of electrospinning parameters on the mechanical and morphological characteristics of small diameter PCL tissue engineered blood vessel scaffolds having distinct micro and nano fibre populations—a DOE approach. *Polymer Testing*, 96, p.107119.
- Pashneh-Tala, S., MacNeil, S. and Claeysens, F. (2016). The tissue-engineered vascular graft—past, present, and future. *Tissue Engineering Part B: Reviews*, 22(1), pp.68-100.
- Paxton, N., Smolan, W., Böck, T., Melchels, F., Groll, J. and Jungst, T. (2017). Proposal to assess printability of bioinks for extrusion-based bioprinting and evaluation of rheological properties governing bioprintability. *Biofabrication*, 9(4), p.044107.
- Pires, A.L.R., Bierhalz, A.C. and Moraes, A.M. (2015). Biomaterials: types, applications, and market. *Química Nova*, 38, pp.957-971.

- Pu, J., Yuan, F., Li, S. and Komvopoulos, K. (2015). Electrospun bilayer fibrous scaffolds for enhanced cell infiltration and vascularization in vivo. *Acta biomaterialia*, 13, pp.131-141.
- Rajzer, I., Kurowska, A., Jabłoński, A., Jatteau, S., Śliwka, M., Ziąbka, M. and Menaszek, E., (2018). Layered gelatin/PLLA scaffolds fabricated by electrospinning and 3D printing-for nasal cartilages and subchondral bone reconstruction. *Materials & Design*, 155, pp.297-306.
- Rensen, S.S.M., Doevendans, P.A.F.M. and Van Eys, G.J.J.M. (2007). Regulation and characteristics of vascular smooth muscle cell phenotypic diversity. *Netherlands Heart Journal*, 15(3), pp.100-108.
- Sharma, P., Kumar, P., Sharma, R., Bhatt, V.D. and Dhot, P.S. (2019). Tissue engineering; current status & futuristic scope. *Journal of medicine and life*, 12(3), p.225.
- Sell, S.A., Wolfe, P.S., Garg, K., McCool, J.M., Rodriguez, I.A. and Bowlin, G.L. (2010). The use of natural polymers in tissue engineering: a focus on electrospun extracellular matrix analogues. *Polymers* 2: 522–553.
- Stefani, I. and Cooper-White, J.J. (2016). Development of an in-process UV-crosslinked, electrospun PCL/aPLA-co-TMC composite polymer for tubular tissue engineering applications. *Acta Biomaterialia*, 36, pp.231-240.
- L'heureux, N., Dusserre, N., Marini, A., Garrido, S., De La Fuente, L. and McAllister, T., (2007). Technology insight: the evolution of tissue-engineered vascular grafts—from research to clinical practice. *Nature clinical practice Cardiovascular medicine*, 4(7), pp.389-395.
- Xu, L., Varkey, M., Jorgensen, A., Ju, J., Jin, Q., Park, J.H., Fu, Y., Zhang, G., Ke, D., Zhao, W. and Hou, R. (2020). Bioprinting small diameter blood vessel constructs with an endothelial and smooth muscle cell bilayer in a single step. *Biofabrication*, 12(4), p.045012.
- Yamanaka, H., Yamaoka, T., Mahara, A., Morimoto, N. and Suzuki, S. (2018). Tissue-engineered submillimeter-diameter vascular grafts for free flap survival in rat model. *Biomaterials*, 179, pp.156-163.
- Yang, Y., Lei, D., Zou, H., Huang, S., Yang, Q., Li, S., Qing, F.L., Ye, X., You, Z. and Zhao, Q. (2019). Hybrid electrospun rapamycin-loaded small-diameter decellularized vascular grafts effectively inhibit intimal hyperplasia. *Acta biomaterialia*, 97, pp.321-332.
- Yuan, H., Zhou, Q. and Zhang, Y. (2017). Improving fiber alignment during electrospinning. *Electrospun nanofibers*, pp.125-147.
- Zhang, Y.S., Oklu, R., Dokmeci, M.R. and Khademhosseini, A. (2018). Three-dimensional bioprinting strategies for tissue engineering. *Cold Spring Harbor perspectives in medicine*, 8(2), p.a025718.
- Zhu, J., Chen, D., Du, J., Chen, X., Wang, J., Zhang, H., Chen, S., Wu, J., Zhu, T. and Mo, X. (2020). Mechanical matching nanofibrous vascular scaffold with effective anticoagulation for vascular tissue engineering. *Composites Part B: Engineering*, 186, p.107788.
- Zoghbi, W.A., Duncan, T., Antman, E., Barbosa, M., Champagne, B., Chen, D., Gamra, H., Harold, J.G., Josephson, S., Komajda, M. and Logstrup, S. (2014). Sustainable development goals and the future of cardiovascular health: a statement from the global cardiovascular disease taskforce. *Journal of the American Heart Association*, 3(5), p.e000504.